LA-UR- 09-01137

Approved for public release; distribution is unlimited.

Title:	Sub-picosecond optical switching with a negative-index metamaterial
Author(s):	K. M. Dani Zahyun Ku Prashanth C. Upadhya Rohit P. Prasankumar S. R. J. Brueck Antoinette J. Taylor
Intended for:	Nature Photonics

Los Alamos
NATIONAL LABORATORY
EST. 1943

Form 836 (7/06)

Sub-picosecond optical switching with a negative index metamaterial

K. M. Dani[1], Zahyun Ku[2], Prashanth C. Upadhya[1], Rohit P. Prasankumar[1], S.R.J. Brueck[2] and Antoinette J. Taylor[1]

[1]Center for Integrated Nanotechnologies, Los Alamos National Laboratory, Los Alamos, NM 87545,
[2]Center for High Technology Materials and Electrical and Computer Engineering Dept., Univ. of New Mexico
Tel. 505 665 8839, Fax 505 665 9030, Email: KMDani@lanl.gov

Development of all-optical signal processing, eliminating the performance and cost penalties of optical-electrical-optical conversion, is important for continuing advances in Terabits/sec (Tb/s) communications.[1] Optical nonlinearities are generally weak, traditionally requiring long-path, large-area devices[1,2] or very high-Q, narrow-band resonator structures.[3] Optical metamaterials offer unique capabilities for optical-optical interactions. Here we report 600 femtosecond (fs) all-optical modulation using a fishnet (2D-perforated metal/amorphous-Si (α-Si)/metal film stack) negative-index metamaterial with a structurally tunable broad-band response near 1.2 μm. Over 20% modulation (experimentally limited) is achieved in a path length of only 116 nm by photo-excitation of carriers in the α-Si layer. This has the potential for Tb/s all-optical communication and will lead to other novel, compact, tunable sub-picosecond (ps) photonic devices.

Due to generally weak ($[\chi^{(2)}]^2$ or $\chi^{(3)}$) optical nonlinearities, all-optical Kerr-effect and three/four-wave mixing modulators require macroscopic propagation lengths, from cm's in the case of periodically-poled $LiNbO_3$ (PPLN)[4] to km for fiber approaches.[1] Semiconductor optical amplifiers (SOA) offer larger nonlinearities, but these are active devices adding optical noise and requiring significant additional area for carrier injection and heat dissipation.[1] High-Q crystalline semiconductor structures, modulated by optical carrier injection, are inherently slow as a result of long carrier lifetimes.[3] Very recently, 200 fs modulation ($\Delta T/T$ ~ 8% for a ~ 100 μm propagation/coupling length) of a propagating surface plasma wave was achieved utilizing a non-linear surface plasmon-light interaction.[5] In contrast, here we use a metamaterial device to demonstrate ~ 600 fs modulation in the near-infrared (NIR) with > 20% depth in a propagation length of only 116 nm.

Metamaterials are a new class of nanostructured materials that offer novel optical properties such as a negative index of refraction. To date, much effort has been devoted to the fabrication of these materials and the characterization of their linear optical properties; and to extending the wavelength range to the NIR and visible.[6] However, only limited results have been presented on modulation of these properties in the THz[7,8] (~ 20 ps response) and NIR[9] (~ 60 ps response) spectral regions. In these reports, as in this work, the metamaterial includes a sub-wavelength LC resonance tank circuit, with metal and semiconductor components, yielding negative permeability. Here, we use optical carrier injection to modify the conductivity of the semiconductor and dynamically affect the resonance behavior. A 116 nm thick Ag/α-Si/Ag fishnet structure is used to take advantage of the fast carrier recombination in the non-crystalline α-Si. An experimentally limited transmission modulation $\Delta T/T$ of up to ~20% with an ultrafast response time of ~ 600 fs

is observed in a fs-pump-probe experiment. Qualitative agreement with FDTD simulations is obtained. The sub-ps pump-probe response has the potential for all-optical Tb/s communication, while the nm-scale thickness results in a compact device easily integrated with other photonic devices and applications. Further, by scaling metamaterial dimensions one can tune the device response over the NIR spectrum leading to a tunable, compact sub-picosecond photonic device.

The metamaterial structure (Fig. 1) is composed of two 28 nm thick silver films separated by a 60 nm thick α-Si film. A two-dimensional square periodic array of elliptical holes penetrates all three layers, providing an elliptical negative index metamaterial (eNIM). Figure 2 shows the measured transmission of this structure along with the modeled transmission (FDTD) and the effective refractive index for light polarized with the E-field parallel to the thinnest metal lines (Fig. 1). The longer wavelength negative-index resonance, previously reported in similar structures,[10] is at ~1.68 μm. There is a second, shorter wavelength negative-*n* resonance at ~ 1.13 μm. The wavelength ratio of the two resonances, $\sim\sqrt{2}$, suggests that the long wavelength resonance is associated with the periodicity of the holes (p = 340 nm) while the shorter one is associated with the periodicity along the diagonals ($\sim p/\sqrt{2} \sim 240$ nm). This identification is confirmed by the FDTD modeling. Figure 3 shows the simulated magnetic field strength at the two resonances with the periodicities indicated. As an aside this result suggests that the fishnet structure is not a "true" metamaterial in the sense that the resonances are not independent of the periodicity. This is consistent with the observation that the negative permeability is associated with periodic nanostructure coupling to the gap-mode surface plasma wave between the two metal films.[11]

To study the ultrafast modulation of the optical properties of the eNIM, a sub-100 fs, visible pump was used to photoexcite carriers above the α-Si bandgap (~731 nm); and the time-resolved change in transmission was measured with a near-IR probe pulse. The pump-induced percentage change in transmission ($\Delta T/T$), i.e. switching ratio, is measured as a function of pump-probe delay (Δt), pump fluence, pump wavelength, probe wavelength (1.0-1.5 μm) and probe polarization. The incident pump fluence at the sample was experimentally limited to 1.35 mJ/cm^2 (for 450 to 700 nm) and 3.9 mJ/cm^2 at 400 nm.

Due to the elliptical holes in the metamaterial, there is a strong negative index resonance only for one polarization. Correspondingly, a strong pump-probe signal is observed only for that probe polarization and the response is about an order of magnitude smaller for the other probe polarization. In Fig. 4 the metamaterial $\Delta T/T$ versus pump-probe delay at three different pump fluences is plotted. Here, the pump (probe) is at 550 nm (1180 nm). The dashed lines show a numerical fit to the data using a triple exponential decay convoluted with a Gaussian to account for the 120 fs rise time, which corresponds to the finite width of the pump-probe cross-correlation. A fast 600 fs component, an intermediate few-picosecond component, and a slow nanosecond component are observed. The nanosecond decay time cannot be resolved within the limitations of our experiment and is accounted for as a constant negative background. The inset shows the peak switching ratio versus pump fluence and the contributions of each component as extracted from the nu-

merical fits. Over 80% of the signal amplitude is due to the fast 600 fs component, which increases rapidly with pump fluence. A $\Delta T/T$ of ~ 20% was obtained at the highest available 550 nm pump fluence of 1.35 mJ/cm^2. Pumping at 400 nm with ~2.5 mJ/cm^2 resulted in 40% switching ratios. However, the 400 nm pump degraded the Ag layer of the sample over time due to the strong metal absorption at 400 nm. The solid yellow curve shows the magnified pump-probe signal from an unstructured 60 nm α-Si film for comparison. A triple exponential decay (dashed line) fits the curve well with a fast sub-picosecond component, an intermediate few-picosecond component and a slow component that lasts for > 100 ps . Previous studies on ultrafast carrier dynamics in α-Si have explained such multi-component decay times[12-15] on the basis of processes including Auger recombination,[14] trapping of free carriers into defect states, and intraband migration and recombination.[15] The close correspondence of the fast and intermediate decay-time components of α-Si and the metamaterial suggests that the change in optical properties of the metamaterial is the result of the dynamics of the photoexcited carriers in the dielectric α-Si layer. Further, an unstructured 28 nm film of Ag shows no measurable pump-probe signal under identical conditions.

In Fig. 5a, the metamaterial pump-probe signal is plotted at different probe wavelengths for a 550 nm 1.35 mJ/cm^2 excitation. At zero pump-probe delay (Δt = 0), the peak switching ratio goes from positive to negative as the probe is moved to shorter wavelengths relative to the negative index resonance. Additionally, for a fixed probe wavelength, the pump-probe signal changes from positive to negative (or vice versa) as the pump-probe delay is increased. Around the 1130 nm negative-index resonance, we observe a sub-ps change in $\Delta T/T$ from negative to positive. Since photoexcitation of α-Si changes both the real and the imaginary parts of the refractive index, which in turn tune the negative index resonance, the data is suggestive of a dynamic ultrafast tuning of the negative index resonance.

To understand these experimental results, the optical properties of the metamaterial were simulated using a commercial 3D FDTD solver (CST Microwave Studio).[16] Both perfect electric conductor and perfect magnetic conductor boundary conditions at the edges of the unit cell are used to model a TEM plane wave propagating through the metamaterial with the specific polarization direction shown in Fig. 1a. We take the refractive index of un-photoexcited α-Si, $n_{\alpha\text{-Si}}$ = 3.4 and $n_{substrate}$ = 1.5. For photoexcited α-Si, the Drude model[17] gives,

$$n_{photoexcited\ \alpha-Si} = n_{\alpha-Si}\left[1-\frac{\omega_p^{\ 2}}{\omega(\omega+i\gamma_m)}\right]^{1/2},$$

where $\omega_p = \left[e^2N/\varepsilon_0 m^*\right]^{1/2}$ is the plasma frequency, ω – angular frequency of probe light, m^* – effective mass, ε_0 – permittivity of free space, N – photoexcited carrier density and γ – the scatering rate. Only the electronic contribution is considered given the larger effective mass[12,18] and lower mobility[12,19] for holes. For a pump fluence of 1.35 mJ/cm^2, $N = 1.8\times10^{20}\,cm^{-3}$. We relate γ to the free carrier mobility by $\gamma^{-1} = e/\mu m^*$ [20]. For $m^* = 0.2m_0$ [12,18,21] and μ = 10 cm^2/Vs,[12,18,19] we get γ^{-1}~1 fs[12,21,22] and $n_{photoexcited\ \alpha\text{-Si}}$ = 3.27 + i0.08. For the silver dielectric function, the Drude model is described by ω_p = 9.02 eV

Formatted: Endnote Reference, Font: (Default) Times New Roman
Deleted: [14]
Formatted: Endnote Reference, Font: (Default) Times New Roman
Deleted: [15]
Formatted: Endnote Reference, Not Superscript/ Subscript
Deleted: [12]
Deleted: [12]
Formatted: Endnote Reference, Not Superscript/ Subscript
Deleted: [18]
Deleted: [19]
Formatted: Endnote Reference, Not Superscript/ Subscript
Deleted: [12]
Deleted: [12]
Formatted: Endnote Reference, Not Superscript/ Subscript
Deleted: [18]
Formatted: Endnote Reference, Not Superscript/ Subscript
Deleted: [12]
Formatted: Endnote Reference, Not Superscript/ Subscript
Formatted: Endnote Reference, Not Superscript/ Subscript
Deleted: [21]
Formatted: Endnote Reference, Not Superscript/ Subscript

and $\gamma = 0.052$ eV, where γ is a factor of 2.5 larger than reported for bulk materials to account for additional thin-film scattering and fabrication inhomogeneity.[23]

Fig. 5b shows the calculated transmittance of the metamaterial versus wavelength with and without photoexcitation. As the α-Si layer turns conductive with increasing photoexcitation, the transmittance of the metamaterial changes from that of a negative index material to a more metallic plasmonic response. The inset shows the calculated switching ratio versus wavelength, qualitatively reproducing the measured switching ratio at zero pump-probe delay.

In conclusion, ultrafast (600 fs) optical switching in a 116-nm thick negative index metamaterial has been demonstrated. This effect has the potential for over 1 Tb/s all-optical signal processing – a significant improvement over current technology. This study suggests the possibility of other compact and tunable photonic devices – such as frequency tuners and phase modulators – where the novel optical properties of negative-index materials can be manipulated on a sub-ps timescale.

METHODS AND PROCEDURE

METAMATERIAL FABRICATION:

The processing steps for the elliptical negative-index metamaterials were as follows. (I) BK7 glass substrate (2.5x2.5 cm^2) was cleaned with piranha solution with a volume concentration ratio of H_2SO_4/H_2O_2 of 4:1 to remove any residual organic contamination, followed by dehydration. Polymethyl methacrylate (MicroChem: 950 PMMA 2% in Anisole) was spun onto the substrate as a sacrificial layer for liftoff processing in the final step (see V below). A bottom anti-reflection coating (BARC) (Brewer Science: XHRIC-16) for i-line lithography, followed by negative-tone photoresist (Futurrex: NR7-500P) were then deposited by spinning and baked. (II) Interferometric lithography[24] using a 355-nm third harmonic YAG:Nd^{3+} laser source was carried out to produce a periodic elliptical hole pattern in the photoresist layer with two successive orthogonal 1D exposures with different doses (for the elliptical holes), then developed (MF702). (III) A 25-nm thick layer of chromium (Cr) as a selective etch mask was deposited on the developed sample using e-beam evaporation, followed by a liftoff processing with acetone to remove the PR layer. During this liftoff, the PMMA layer was protected by the layer of BARC. The result was an array of elliptical Cr dots atop the BARC layer. (IV) A predominately anisotropic O_2 plasma reactive-ion-etch (RIE) at RF power (200W), O_2 gas (50 sccm) and O_2 pressure (200 mT) with slight isotropic component was used to etch through the BARC and PMMA to the substrate while generating a small undercut for the subsequent liftoff process. (V) Consecutive e-beam evaporations were used to deposit Ag/α-Si/Ag. (VI) Liftoff processing using the PMMA sacrificial layer with acetone was carried out to remove the Ag/α-Si/Ag on top of Cr/BARC/PMMA posts. This last step was different from previous work, which used a high pressure, isotropic O_2 plasma ash to remove the posts, since the O_2 plasma ash can potentially damage the Ag metal surface. (VII) A final 30-nm thick, blanket, e-beam deposited magnesium fluoride (MgF_2) layer served as a protection layer, isolating the Ag from oxidation during optical pumping.

OPTICAL PUMP-PROBE MEASUREMENTS

A 100 kHz regenerative amplifier producing sub-60 fs, 800 nm wavelength pulses is used to simultaneously seed visible and NIR optical parametric amplifiers (OPA). The signal output of the visible OPA (450 to 700 nm) or the residual, frequency-doubled 400 nm pulses from the amplifier provide the pump pulses; while the output of the NIR OPA provides the probe pulses. The pump is focused onto the sample at a ~20° angle with a spot size of ~100 μm. The probe fluence at the sample is kept below 10% of the pump fluence, and the normally incident probe was focused down to a spot size of about 30 μm so as to sample only the central uniformly photoexcited region of the metamaterial.

---

[1] Saruwatari, M. All-optical signal processing for terabit/second optical transmission. *IEEE Jour. Sel. Top. In Quant. Elec.* **6**, 1363-1374 (2000).

[2] Hochberg, M., et al. Terahertz all-optical modulation in a silicon-polymer hybrid system. *Nature Materials* **5**, 703-709 (2006).

[3] Manolatou, C. & Lipson, M. All-optical silicon modulators based on carrier injection by two-photon absorption. *Jour. Lightwave Tech.* **24**, 1433-1439 (2006).

[4] Langrock, C., Kumar, S., McGeehan, J. E., Willner A. E. & Fejer, M. M. All-Optical Signal Processing using $\chi^{(2)}$ Nonlinearities in Guided Wave Devices. *Jour. Lightwave Tech.* **24**, 2579-2592 (2006).

[5] MacDonald, K. F., Samson, Z. L., Stockman, M. I., Zheludev, N. I. Ultrafast Active Plasmonics. *Nature Photonics* **3,** 55-58 (2009).

[6] Shalaev, V. M. Optical negative-index metamaterials. *Nature Photonics* **1**, 41-48 (2007).

[7] Padilla, W. J., Taylor, A. J., Highstrete, C., Lee, M., & Averitt, R. D. Dynamical Electric and Magnetic Metamaterial Response at Terahertz Frequencies. *Phys. Rev. Lett.* **96,** 107401 (2006).

[8] Chen, H. T., et al. Ultrafast optical switching of terahertz metamaterials fabricated on ErAs/GaAs nanoisland superlattices. *Opt. Lett.* **32,** 1620 (2007).

[9] Kim, E. et al., Modulation of negative index metamaterials in the near-IR range. *Appl. Phys. Lett.* **91,** 17305 (2007).

[10] Zhang, S., et al. Experimental demonstration of near-infrared negative-index metamaterials. *Phys. Rev. Lett.* **95,** 137404 (2005).

[11] Mary, A., Rodrigo, S. G., Garcia-Vidal, F. J. & Martín-Moreno, L. Theory of negative-refractive-index respone of double fishnet structures. *Phys. Rev. Lett.* **101,** 103902 (2008).

[12] Fauchet, P. M., Hulin, D., Vanderhaghen, R., Mourchid, A. & Nighan, W. L. Jr. The properties of free carriers in amorphous silicon. *J. of Non-Cryst. Solids* **141,** 76-87 (1992)

[13] Mourchid, A., Vanderhaghen, R., Hulin, D., Tanguy, C. & Fauchet, P. M. Femtosecond optical spectroscopy in a-Si:H and its alloys. *J. of Non-Cryst. Solids* **114,** 582-584 (1989)

[14] Esser, A., et al. Ultrafast recombination and trapping in amorphous silicon. *Phys. Rev. B* **41,** 2879-2884 (1990)

[15] Shkrob, I. A. & Crowell, R. A. Ultrafast charge recombination in undoped amorphous hydrogenated silicon. *Phys. Rev. B* **57,** 12207-12218 (1998)

[16] CST Studio Suite 2006B, <www.cst.com>

[17] Dressel, M. & Gruner, G. *Electrodynamics of Solids* Ch. 5 (Cambridge Univ. Press, New York, NY, 2002)

[18] Pankove, J. I. *Hydrogenated Amorphous Silicon* (Academic Press, Orlando, FL, 1984)

[19] Street, R. A. *Hydrogenated Amorphous Silicon* (Cambridge Univ. Press, New York, NY, 1991)

[20] Singleton, J. *Band Theory and Electronic Properties of Solids* Ch. 9.3 (Oxford Univ. Press, New York, NY, 2001)

[21] Choi, T. Y., Hwang, D. J. & Grigoropoulos, C. P. Ultrafast laser-induced crystallization of amorphous silicon films. *Opt. Eng.* **42,** 3383-3388 (2003)

[22] Sokolowski-Tinten, K. & Von der Linde, D. Generation of dense electron-hole plasmas in silicon. *Phys Rev. B* **61,** 2643-2650 (2000)

[23] Ku, Z. & Brueck, S. R. J. Comparison of negative refractive index materials with circular, elliptical and rectangular holes. *Opt. Express* **15,** 4515 (2007).

[24] Brueck, S. R. J. Optical and Interferometric Lithography – Nanotechnology Enablers. *Proc. IEEE* **93,** 1704 (2005)

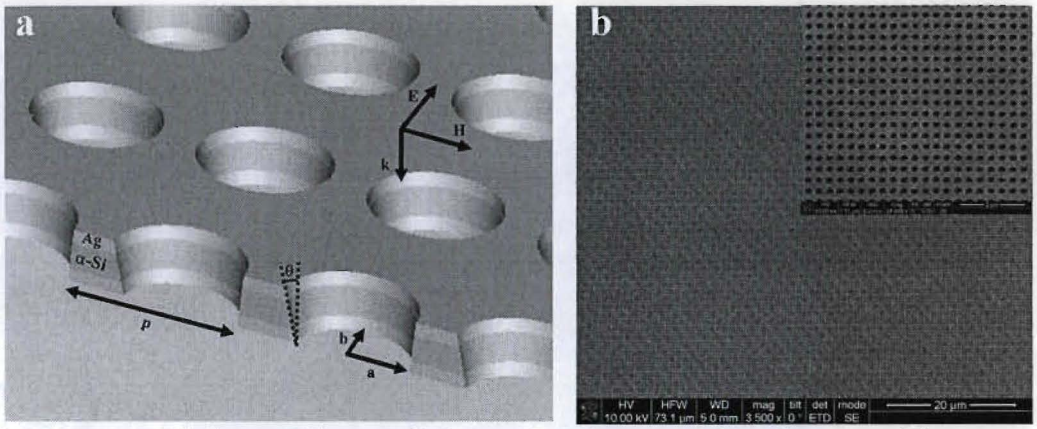

Fig 1 Diagram and SEM image of fabricated elliptical negative-index metamaterials. a. Geometry and dimensions of elliptical negative-index metamaterials: p = 340 nm; $2a$ = 227 nm; $2b$ = 164 nm and θ (sidewall-angle) = 8°. The structure constitutes 3 alternating layers of 28 nm thick silver (Ag) and 60 nm thick amorphous silicon (α-Si). In addition, the configuration of polarization and propagation is depicted (E, H and k denote electric field, magnetic field and wave vector, respectively). b. Top view SEM image of the 3 layered elliptical NIMs.

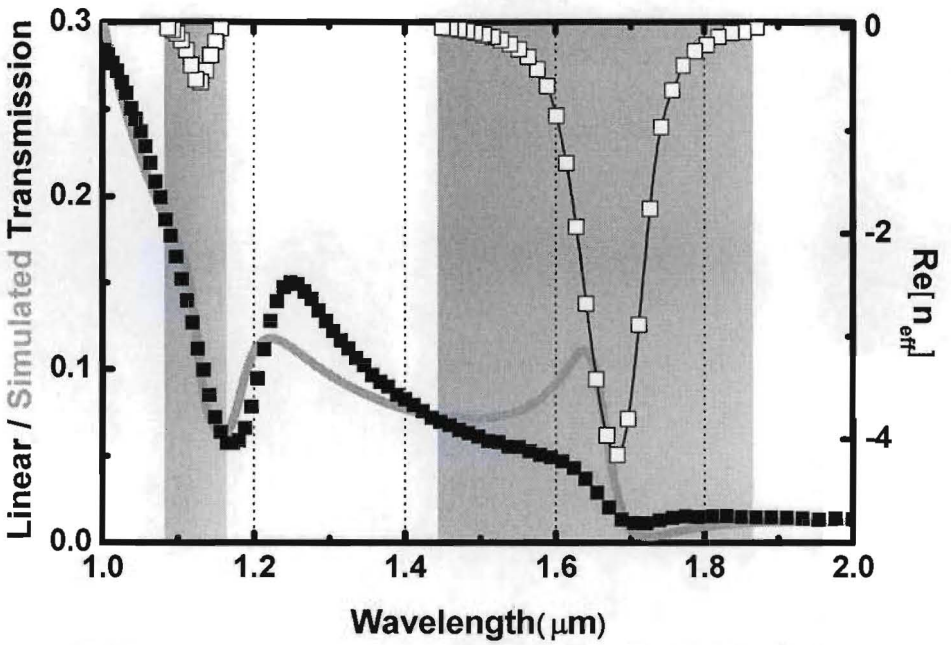

Fig. 2. Experimental normal incidence transmission spectrum (FTIR) with polarization direction indicated in Fig. 1. The simulated transmission curve is obtained with CST Microwave Studio, which gives a good fit to measured transmission using 2.5 times the scattering frequency of bulk silver. The shaded areas represent wavelength regions of negative refractive index as shown (FDTD simulation). The simulation is optimized for the region ~ 1.15 μm where the high-speed measurements are made.

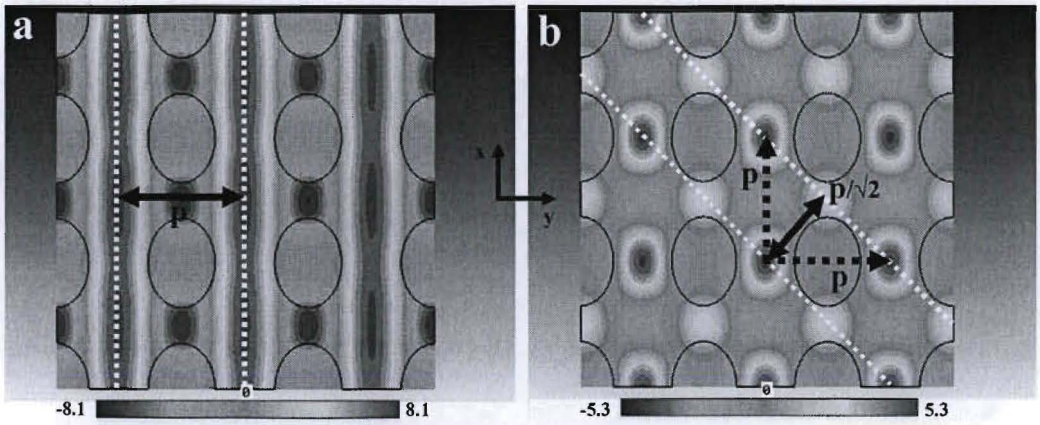

Fig. 3. The simulated magnetic field distribution for elliptical negative-index metamaterials in the *x*,*y* plane through middle of structure at the corresponding resonant frequencies (a. lower frequency, b. higher frequency).

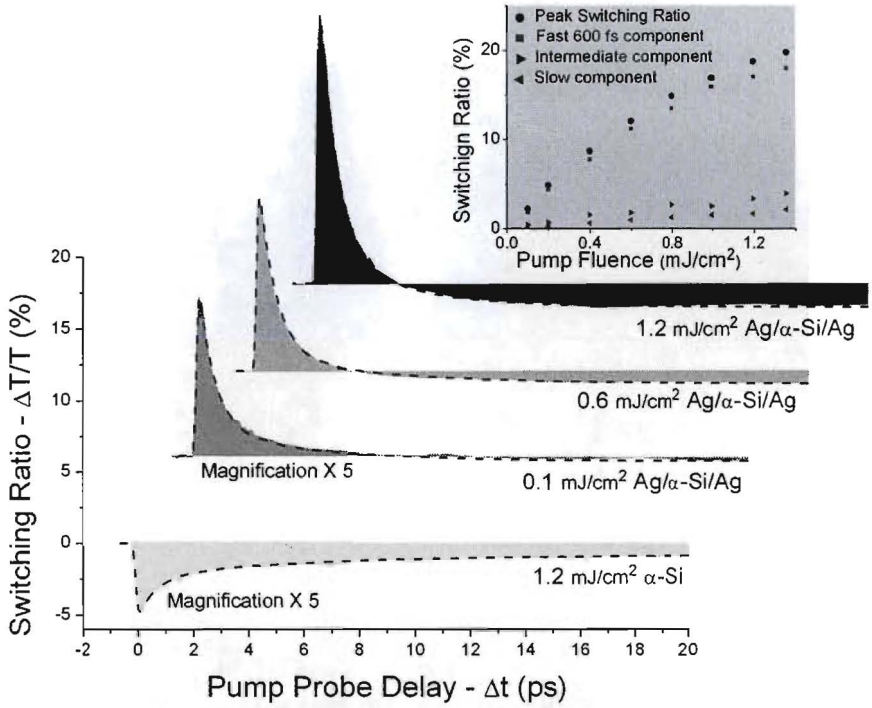

Fig. 4: Comparison of pump-probe signal decay times for the eNIM and an unstructured α-Si film [pump (probe) wavelength 550 (1180) nm]. The data (solid colors) is fit to a triple exponential decay convoluted with a Gaussian (dashed lines). (X-offset = 2.2 ps; Y-offset = 6%) We see a fast 600 fs component, an intermediate few-picosecond component and a slow nanosecond component. Inset: Peak switching ratio and amplitudes of each component versus fluence.

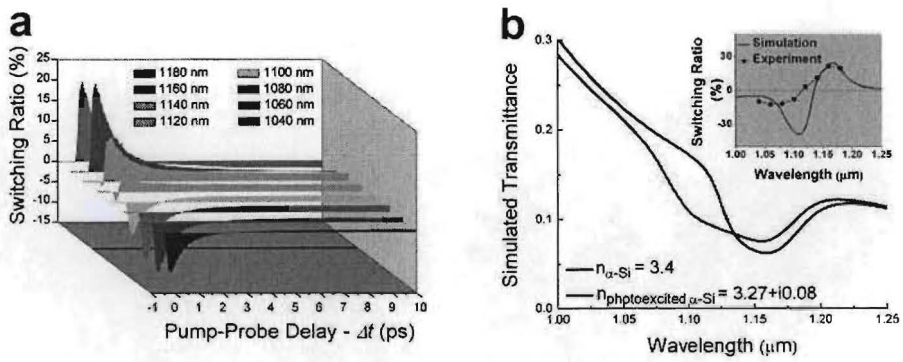

Fig 5. eNIM pump-probe signal at different probe wavelengths (550 nm pump wavelength). (a) Experimental data versus pump-probe delay. (b) Simulated transmittance for photoexcited and un-photoexcited eNIM. Inset: Simulated switching ratio versus probe wavelength compared with that measured at zero pump-probe delay.